Enhanced telecom wavelength single-photon detection with NbTiN superconducting nanowires on oxidized silicon

M. G. Tanner,[1,a)] C. M. Natarajan,[1] V. K. Pottapenjara,[1] J. A. O'Connor,[1] R. J. Warburton,[1] R. H. Hadfield,[1] B. Baek,[2] S. Nam,[2] S. N. Dorenbos,[3] E. Bermúdez Ureña,[3] T. Zijlstra,[3] T. M. Klapwijk,[3] and V. Zwiller[3]

[1]*Scottish Universities Physics Alliance and School of Engineering and Physical Sciences, Heriot-Watt University, Edinburgh EH14 4AS, United Kingdom*

[2]*National Institute of Standards and Technology, 325 Broadway, Boulder, Colorado 80305, USA*

[3]*Kavli Institute for Nanoscience, Delft University of Technology, Lorentzweg 1, 2628 CJ Delft, The Netherlands*

(Received 10 February 2010; accepted 21 April 2010; published online 3 June 2010)

Superconducting nanowire single-photon detectors (SNSPDs) have emerged as a highly promising infrared single-photon detector technology. Next-generation devices are being developed with enhanced detection efficiency (DE) at key technological wavelengths via the use of optical cavities. Furthermore, new materials and substrates are being explored for improved fabrication versatility, higher DE, and lower dark counts. We report on the practical performance of packaged NbTiN SNSPDs fabricated on oxidized silicon substrates in the wavelength range from 830 to 1700 nm. We exploit constructive interference from the SiO_2/Si interface in order to achieve enhanced front-side fiber-coupled DE of 23.2 % at 1310 nm, at 1 kHz dark count rate, with 60 ps full width half maximum timing jitter. © *2010 American Institute of Physics*. [doi:10.1063/1.3428960]

Infrared single-photon detectors are a key enabling technology for a host of scientific applications. Advanced photon-counting applications place stringent demands on detector performance, and new detector technologies are rapidly being developed, evaluated, and deployed.[1] Superconducting nanowire single-photon detectors (SNSPDs) (Refs. 2–4) offer wide spectral range (from visible to midinfrared wavelengths) with free-running operation, low dark counts, short reset times, and low timing jitter. SNSPDs have begun to have a significant impact on applications, such as quantum key distribution,[5] time-of-flight ranging,[6] high bit-rate ground-to-space communications,[7] and optical quantum information processing.[8] Recent work on SNSPDs has concentrated on increasing detection efficiency (DE) through improved materials, device layout, and optical architecture.[3,4,9–12] Optical cavities increase the absorption of photons in the active device layer[9–11] and nanopositioning systems are employed to maximize coupling efficiency to the device area.[12]

The ~1300 nm wavelength range is important for quantum information experiments using telecom-wavelength quantum-dot single-photon sources[13] and medical applications such as singlet oxygen detection at $\lambda = 1273$ nm.[14] In this paper we report on enhanced device efficiency in a NbTiN SNSPD (Ref. 15) with a cavity reflection from the oxidized Si substrate optimized for ~1300 nm wavelength. The devices are front-side fiber-coupled in a fixed package without the need for nanopositioners or thinning of the substrate used in backside illumination architectures.[9,10,12] In this paper, we describe device performance as a function of wavelength, with reference to the device architecture. We demonstrate the highest published efficiency in a practically packaged SNSPD at $\lambda = 1310$ nm with frontside fiber illumination, comparable to results achieved with backside illumination.

Devices used in this study[15] are based on high quality films of NbTiN deposited by reactive dc magnetron sputtering at room temperature on a Si substrate with a 225 nm SiO_2 layer.[16] Further device fabrication details are given in Ref. 15. The devices studied consist of a 10×10 μm^2 detector, composed of a meander wire 100 nm wide with 200 nm pitch. This was aligned to a single-mode optical fiber (9 μm mode field diameter) as shown in Fig. 1(a). The chip-to-fiber spacing was determined through white-light interferometry ($d = 35$ μm, at room temperature decreasing to $d < 10$ μm at the operating temperature of 2.8 K).

Electrical and optical testing is performed in a Gifford–McMahon cryocooler at a device temperature of 2.8 K, well below the observed device superconducting transition temperature of ~8 K. The experimental arrangement for DE measurements is shown in Fig. 1(d). The optical attenuation of the laser diode source is varied to control the photon flux while the detector count rate is monitored. Bias current is varied to control the dark counts. System DE (determined from the fiber input to the cryostat) was measured by use of calibrated laser diodes at 830, 1310, and 1550 nm wavelength with polarization optimized for both high and low device DE (Ref. 17) at multiple biasing points, as shown in Fig. 2. High DE is observed at all wavelengths, at 1 kHz dark count rate DE=8.5%, 23.2%, and 7.8% at 830 nm, 1310 nm and 1550 nm wavelength, respectively. At dark count rates as low as 20 Hz, DE of 7.5 %, 10%, and 2.8% are observed for 830 nm, 1310 nm and 1550 nm illumination, respectively. The most striking feature is that DE is higher at 1310 than 830 or 1550 nm wavelength owing to the optical structure (discussed below). Without an optical cavity, efficiency will decrease with increasing wavelength.[3] In other respects, the DE versus dark count rate conforms to behavior observed in NbN SNSPDs.[18] When dark count rate is reduced from

a)Electronic mail: m.tanner@hw.ac.uk.

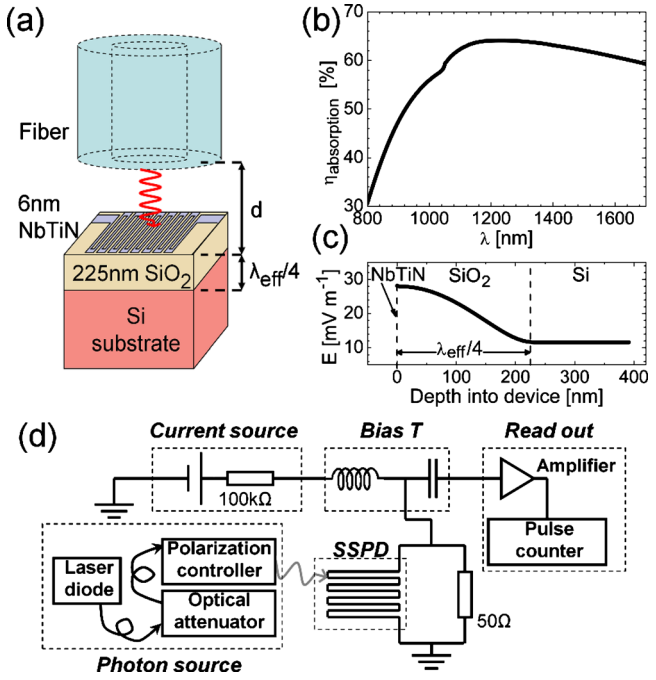

FIG. 1. (Color online) (a) Full chip and fiber arrangement, not to scale. (b) Simulated probability of photon absorption in NbTiN layer ($\eta_{absorption}$). (c) Simulated electric field in device layers assuming 10^6 photons incident in a 10×10 μm^2 device area with $\lambda=1310$ nm. (d) Experimental arrangement for DE measurements. Current is supplied below I_c through the dc line of the bias T, while pulses are read out through the ac line. Laser diodes of different wavelengths are attenuated to provide a controlled photon flux (via calibrated in-fiber attenuation). A manual polarization controller is used to match the optimum photon polarization to the device orientation.

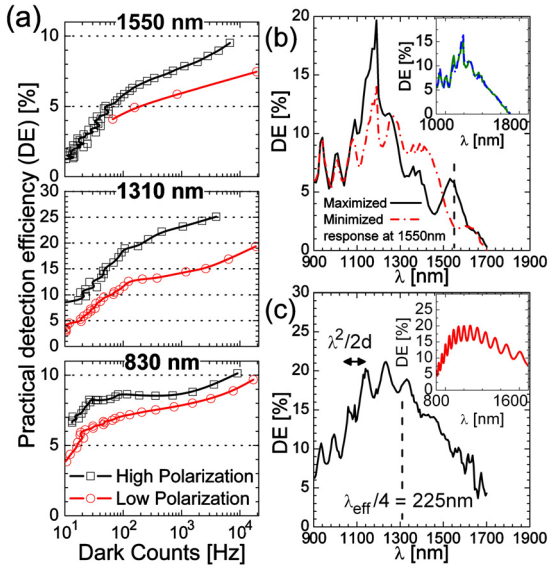

FIG. 2. (Color online) (a) Device detection efficiency vs dark count rate at three wavelengths. Polarization optimized for high (low) efficiency shown as squares (circles). Note: vertical scales vary. (b) Polarization-dependent measurement of DE over a wide wavelength range with 700 Hz dark count rate. (Main plot) Detection efficiency with fixed input polarization set to maximize (minimize) response at 1550 nm shown as solid (dashed) line. (Inset) Average of the two results from the main plot shown as dashed line. Data taken with the polarization scrambling method shown as solid line precisely aligning with the averaged data. (c) DE with varying wavelength at 1.7 kHz dark count rate. (Main plot) Average of measurements taken with polarization set for high and low response at reference wavelengths to produce a polarization independent result. Vertical dashed line marks the designed absorption maximum. (Inset) Simulated data with $\kappa=1$ μm^{-1}.

1 kHz to 20 Hz, the fractional loss in device efficiency is greatest at $\lambda=1550$ nm ($DE_{20\ Hz}/DE_{1\ kHz}=0.36$), and least at $\lambda=830$ nm ($DE_{20\ Hz}/DE_{1\ kHz}=0.88$). At shorter wavelengths, photons have sufficient energy to trigger an output pulse even at low bias current.[3,19]

Inductance and timing jitter are important performance parameters in SNSPDs. The absolute kinetic inductance value L_K sets the recovery time of the device.[20,21] Inductance measured as a function of bias, using a vector network analyzer, indicates device uniformity.[22] L_K of 342 nH was measured at zero bias current, which agrees well with observed pulse decay time (1/e) of 6.58 ns. A 25% upturn in L_K was observed toward I_c. This supports the observation of high DE and indicates that film quality and wire fabrication are extremely uniform. The jitter of the device is the timing uncertainty between the photon arrival and the electrical output pulse, and limits how accurately events can be time-stamped. Measurements at $\lambda=1550$ nm using a 50 ps full width at half maximum (FWHM) diode laser and a time-correlated single-photon counting card, gave ~60 ps FWHM jitter, comparable to other 10×10 μm^2 NbN SNSPDs.[23]

DE can be defined as $DE=\eta_{coupling}\cdot\eta_{absorption}\cdot\eta_{pulse}$, where $\eta_{coupling}$ is the optical coupling probability, $\eta_{absorption}$ is the probability of photon absorption in the NbTiN layer, and η_{pulse} is the probability of an absorbed photon resulting in a measured pulse.[3,17] In this device, a half cavity is achieved due to the 225 nm SiO_2 ($n\sim1.45$ at $\lambda=1310$ nm) atop the Si substrate ($n\sim3.5$ at $\lambda=1310$ nm). Transfer matrix simulations of multilayer reflectivity are used to calculate the absorption of the NbTiN layer, as shown in Fig. 1(b), giving a clear peak at $\lambda\sim1310$ nm ($\eta_{absorption}\sim65\%$). This corresponds to a SiO_2 layer optical thickness of $\lambda_{eff}/4$ giving an electric field maximum at the NbTiN layer [Fig. 1(c)]. This matches well with the experiment (Fig. 2) in which photons at $\lambda=1310$ nm were detected more efficiently than those at 830 or 1550 nm. Without the cavity reflector, $\eta_{absorption}$ is calculated to be less than ~15% at $\lambda=1310$ nm; thus the layer structure has significantly increased efficiency in the device. While the cavity is not optimized for $\lambda=830$ and 1550 nm, these efficiencies are also increased by the reflection. Without the cavity enhancement (~4× at $\lambda=1310$ nm), the device would demonstrate efficiencies comparable to those of NbN devices.[18] However NbTiN has shown favorable dark count characteristics and is more versatile in growth conditions enabling the fabrication of the cavity devices.[15] It should be noted that the simulations are based on the optical properties of an unpatterned 10 nm thick NbTiN film measured by ellipsometry at room temperature. The real and imaginary parts of the refractive index (n,k) are $n=4.17$ and $k=5.63$ at $\lambda=1310$ nm. This simulation may not link accurately to the absolute absorption in the nanostructured device but reproduces the trend of absorption versus wavelength and the enhancement due to the cavity.

To further test the dependence of DE on wavelength, another NbTiN SNSPD device from the same fabrication batch was fiber-coupled and measured in a second experimental setup. The fixed-wavelength source in Fig. 1(d) was substituted for a white-light source and monochromator with calibrated filters and in-fiber polarization control to produce full spectrum device measurements. Photon count rate was recorded with constant device biasing as wavelength was varied. However, polarization at the device under test varies

with wavelength due to birefringence in the fibers if the photon source arrangement is kept constant. The measurements in Fig. 2(b) have been used to examine this polarization dependence. In the main plot the polarization controller was used to maximize and minimize counts at a reference input wavelength of 1550 nm (dark counts ~700 Hz). The higher device response is seen to oscillate between the two measurements as polarization at the device progresses when the input wavelength is swept. The two full spectrum sweeps for polarization set at the reference wavelength were averaged to produce the dashed line in the inset plot. An additional data set was taken with the polarization controller replaced by an automatic polarization scrambler, shown as the solid line in the plot. The two data sets in the inset match very well, within the expected variation in the device response. This confirms that this averaging method is sufficient to produce a polarization-independent result when a polarization scrambler is not available. To most clearly observe the effect of the optical cavity on the DE, a higher device biasing was used for the data in Fig. 2(c) (dark counts ~1.7 kHz), as this reduces the variation in η_{pulse} across the wavelength range, making the dependence on $\eta_{\text{absorption}}$ more apparent. A peak in DE is seen at a photon wavelength of approximately 1250 nm, lower than the expected absorption peak at 1310 nm. Additional oscillations are present in the data, with a period increasing from 60 to 150 nm across the full wavelength range. These oscillations are due to Fabry–Perot interference between the fiber end and the device surface with separation of $d \sim 8$ μm. It is expected that DE is dependent on the η_{pulse}. As observed in Fig. 2, DE is more dependent on device biasing for longer wavelength photons ($\lambda = 1550$ nm), thus photon energy should be accounted for in η_{pulse}.

In order to fit the data of Fig. 2(c), we approximate the wavelength dependence of an SNSPD at high bias as $\eta_{\text{pulse}} \propto e^{-\kappa\lambda}$, where κ is a fitting constant.[3] The expected efficiency of the device is then $\text{DE}_{\text{sim}} \propto \eta_{\text{absorption}} \cdot e^{-\kappa\lambda}$ if η_{coupling} is taken to be a constant and the fiber-to-device cavity oscillation is included in $\eta_{\text{absorption}}$. The simulated efficiency dependence on wavelength is shown in the inset of Fig. 2(c) with $\kappa = 1$ μm^{-1}. The form of the experimental response is recreated and fiber-to-device oscillations are accurately reproduced in scale and period. The energy dependence of η_{pulse} reduces the wavelength of peak efficiency and causes a greater drop in efficiency at long wavelengths compared to simulated absorption alone, as observed in the experimental result; κ is chosen to give the best fit to both these features. While the form of the simulated absorption matches that of the experimental result, the features are not precisely aligned; this is likely due to (a) the difficulty of accurately obtaining optical data for thin film NbTiN at low temperature, (b) the optical properties of the nanopatterned device, and (c) a more complex dependence of η_{pulse} on wavelength than that used in this work.

In this paper, we have reported the full characterization of a NbTiN SNSPD with a quarter wavelength cavity reflection optimized for $\lambda = 1310$ nm. We have achieved a well understood increase in DE in a practically packaged front side fiber-coupled system. This gives DE of 23.2% with 1 kHz dark count rate at $\lambda = 1310$ nm, with low DE drop-off at lower dark count rates. This is combined with low jitter and fast reset times suitable for use in a variety of time-correlated single-photon counting experiments. Polarization dependence of the detector has been examined, and a convenient averaging method for producing polarization independent response curves has been demonstrated. Simulation of superconducting layer absorption with the additional effects of photon energy and Fabry–Perot oscillations gives a model of the dependence of detector efficiency on incident photon wavelength that describes all experimental features. The optical architecture is well understood and can be optimized for alternative important wavelengths, such as 1550 nm.

This work is supported by the UK Engineering and Physical Science Research Council. R.H.H. is supported by the Royal Society of London (UK) via a University Research Fellowship. We thank Ryan Warburton and Gerald Buller for assistance with the timing jitter measurements.

[1] R. H. Hadfield, Nat. Photonics **3**, 696 (2009).
[2] G. N. Gol'tsman, O. Okunev, G. Chulkova, A. Lipatov, A. Semenov, K. Smirnov, B. Voronov, A. Dzardanov, C. Williams, and R. Sobolewski, Appl. Phys. Lett. **79**, 705 (2001).
[3] A. Verevkin, J. Zhang, R. Sobolewski, A. Lipatov, O. Okunev, G. Chulkova, A. Korneev, K. Smirnov, G. N. Gol'tsman, and A. Semenov, Appl. Phys. Lett. **80**, 4687 (2002).
[4] S. Miki, M. Fujiwara, M. Sasaki, B. Baek, A. J. Miller, R. H. Hadfield, S. W. Nam, and Z. Wang, Appl. Phys. Lett. **92**, 061116 (2008).
[5] H. Takesue, S. W. Nam, Q. Zhang, R. H. Hadfield, T. Honjo, K. Tamaki, and Y. Yamamoto, Nat. Photonics **1**, 343 (2007).
[6] R. E. Warburton, A. McCarthy, A. M. Wallace, S. Hernandez-Marin, R. H. Hadfield, S. W. Nam, and G. S. Buller, Opt. Lett. **32**, 2266 (2007).
[7] B. S. Robinson, A. J. Kerman, E. A. Dauler, R. O. Barron, D. O. Caplan, M. L. Stevens, J. J. Carney, S. A. Hamilton, J. K. W. Yang, and K. K. Berggren, Opt. Lett. **31**, 444 (2006).
[8] J. Chen, J. B. Altepeter, M. Medic, K. F. Lee, B. Gokden, R. H. Hadfield, S. W. Nam, and P. Kumar, Phys. Rev. Lett. **100**, 133603 (2008).
[9] K. M. Rosfjord, J. K. W. Yang, E. A. Dauler, A. J. Kerman, V. Anant, B. M. Voronov, G. N. Gol'tsman, and K. K. Berggren, Opt. Express **14**, 527 (2006).
[10] S. Miki, M. Takeda, M. Fujiwara, M. Sasaki, and Z. Wang, Opt. Express **17**, 23557 (2009).
[11] B. Baek, J. A. Stern, and S. W. Nam, Appl. Phys. Lett. **95**, 191110 (2009).
[12] X. L. Hu, T. Zhong, J. E. White, E. A. Dauler, F. Najafi, C. H. Herder, F. N. C. Wong, and K. K. Berggren, Opt. Lett. **34**, 3607 (2009).
[13] M. B. Ward, O. Z. Karimov, D. C. Unitt, Z. L. Yuan, P. See, D. G. Gevaux, A. J. Shields, P. Atkinson, and D. A. Ritchie, Appl. Phys. Lett. **86**, 201111 (2005).
[14] M. T. Jarvi, M. J. Niedre, M. S. Patterson, and B. C. Wilson, Photochem. Photobiol. **82**, 1198 (2006).
[15] S. N. Dorenbos, E. M. Reiger, U. Perinetti, V. Zwiller, T. Zijlstra, and T. M. Klapwijk, Appl. Phys. Lett. **93**, 131101 (2008).
[16] N. N. Iosad, B. D. Jackson, S. N. Polyakov, P. N. Dmitriev, and T. M. Klapwijk J. Vac. Sci. Technol. A **19**, 1840 (2001).
[17] V. Anant, A. J. Kerman, E. A. Dauler, J. K. W. Yang, K. M. Rosfjord, and K. K. Berggren, Opt. Express **16**, 10750 (2008).
[18] R. H. Hadfield, M. J. Stevens, S. S. Gruber, A. J. Miller, R. E. Schwall, R. P. Mirin, and S. W. Nam, Opt. Express **13**, 10846 (2005).
[19] E. Reiger, S. Dorenbos, V. Zwiller, A. Korneev, G. Chulkova, I. Milostnaya, O. Minaeva, G. Gol'tsman, J. Kitaygorsky, D. Pan, W. Slysz, A. Jukna, and R. Sobolewski, IEEE J. Sel. Top. Quantum Electron. **13**, 934 (2007).
[20] A. J. Kerman, E. A. Dauler, W. E. Keicher, J. K. W. Yang, K. K. Berggren, G. Gol'tsman, and B. Voronov, Appl. Phys. Lett. **88**, 111116 (2006).
[21] R. H. Hadfield, A. J. Miller, S. W. Nam, R. L. Kautz, and R. E. Schwall, Appl. Phys. Lett. **87**, 203505 (2005).
[22] A. J. Kerman, E. A. Dauler, J. K. W. Yang, K. M. Rosfjord, V. Anant, K. K. Berggren, G. N. Gol'tsman, and B. M. Voronov, Appl. Phys. Lett. **90**, 101110 (2007).
[23] M. J. Stevens, R. H. Hadfield, R. E. Schwall, S. W. Nam, R. P. Mirin, and J. A. Gupta, Appl. Phys. Lett. **89**, 031109 (2006).